

LETTER TO THE EDITOR

# First look with JWST spectroscopy: $z \sim 8$ galaxies resemble local analogues

D. Schaerer<sup>1,2</sup>, R. Marques-Chaves<sup>1</sup>, L. Barrufet<sup>1</sup>, P. Oesch<sup>1,3</sup>, Y. I. Izotov<sup>4</sup>, R. Naidu<sup>5</sup>, N. G. Guseva<sup>4</sup>, G. Brammer<sup>3</sup>

<sup>1</sup> Observatoire de Genève, Université de Genève, Chemin Pegasi 51, 1290 Versoix, Switzerland

<sup>2</sup> CNRS, IRAP, 14 Avenue E. Belin, 31400 Toulouse, France

<sup>3</sup> Cosmic Dawn Center (DAWN), Niels Bohr Institute, University of Copenhagen, Jagtvej 128, København N, DK-2200, Denmark

<sup>4</sup> Center for Astrophysics, Harvard & Smithsonian, 60 Garden Street, Cambridge, MA 02138, USA

<sup>5</sup> Bogolyubov Institute for Theoretical Physics, National Academy of Sciences of Ukraine, 14-b Metrolohichna str., Kyiv, 03143, Ukraine

Accepted for publication in A&A Letters

## ABSTRACT

Deep images and near-IR spectra of galaxies in the field of the lensing cluster SMACS J0723.3-7327 were recently taken in the Early Release Observations program of JWST. Among these, two NIRSpec spectra of galaxies at  $z = 7.7$  and one at  $z = 8.5$  were obtained, revealing for the first time rest-frame optical emission line spectra of galaxies in the epoch of reionization, including the detection of the important [O III] $\lambda$ 4363 auroral line (see JWST PR 2022-035). We present an analysis of the emission line properties of these galaxies, finding that these galaxies have a high excitation (as indicated by high ratios of [O III] $\lambda$ 5007/[O II] $\lambda$ 3727, [Ne III] $\lambda$ 3869/[O II] $\lambda$ 3727), strong [O III] $\lambda$ 4363, high equivalent widths, and other properties which are typical of low-metallicity star-forming galaxies. Using the direct method we determine oxygen abundances of  $12 + \log(\text{O}/\text{H}) \approx 7.9$  in two  $z = 7.7$  galaxies, and a lower metallicity of  $12 + \log(\text{O}/\text{H}) \approx 7.4 - 7.5$  ( $\sim 5\%$  solar) in the  $z = 8.5$  galaxy using different strong line methods. More accurate metallicity determinations will require better data. With stellar masses estimated from SED fits, we find that the three galaxies lie close to or below the  $z \sim 2$  mass-metallicity relation. Overall, these first galaxy spectra at  $z \sim 8$  show a strong resemblance of the emission lines properties of galaxies in the epoch of reionization with those of relatively rare local analogues previously studied from the SDSS. Clearly, the first JWST observations demonstrate already the incredible power of spectroscopy to reveal properties of galaxies in the early Universe.

**Key words.** Galaxies: high-redshift – Galaxies: ISM – Cosmology: dark ages, reionization, first stars

## 1. Introduction

Optical emission line spectroscopy has long provided important insights on the physical composition, properties of the interstellar medium (ISM), and the nature of the ionizing power of galaxies, yielding thus key information to understand many key aspects of galaxy evolution (see review of Kewley et al. 2019). The well-known emission lines of H, He, O, N, S, Ne, and other elements detected in optical galaxy spectra, emitted in the ionized ISM (HII regions primarily) have been detected in nearly one million of galaxy spectra, out to redshifts of  $z \sim 0.5 - 1$  with the Sloan Digital Sky Survey (SDSS, Ahumada et al. 2020). Ground-based near-IR spectroscopy has recently pushed these limits to  $z \sim 1.5 - 3$ , where  $\sim 1500$  measurements of the strongest rest-optical lines have been possible, e.g. with the MOSDEF survey (Kriek et al. 2015), revealing thus ISM properties at cosmic noon (e.g. Förster Schreiber & Wuyts 2020).

The recent launch of the JWST and the spectroscopic capabilities of its multi-object near-infrared spectrograph (NIRSpec) in the opens now a completely new window into the early Universe, where, for the first time, all the “classical” optical diagnostics developed at low- $z$  can be used to study the properties of galaxies over a wide redshift range, from  $z \sim 3$  out to the epoch of reionization ( $z > 6.5$ ).

The first public NIRSpec observations, part of the Early Release Observations (ERO) of JWST, have covered the SMACS

J0723.3-7327 galaxy cluster, providing  $1.8 - 5.2 \mu\text{m}$  spectra of 35 objects in the field. Among those, three galaxies in the epoch of reionization were observed, showing spectacular, rich rest-frame optical emission line spectra of objects at  $z = 7.7$  and  $z = 8.5$  (see JWST Press release 2022-035<sup>1</sup>). We here report the first determination of the metallicity (O/H) of these galaxies, a detailed analysis of their emission line properties, and a comparison with observed properties of low- $z$  emission line galaxies. At the time of revision, the JWST targets have been the object of other studies analysing their emission line spectra and derived properties (see Arellano-Córdova et al. 2022; Brinchmann 2022; Carnall et al. 2022; Curti et al. 2022; Katz et al. 2022; Rhoads et al. 2022; Taylor et al. 2022; Trump et al. 2022).

## 2. Observations

### 2.1. JWST NIRSpec observations

Rest-frame UV and optical spectra were obtained on 30 June 2022 using NIRSpec with the micro-shutter assembly (MSA). Observations consist of two different pointings (s007 and s008), each of them using two grating/filter combinations: G235M/F170LP and G395M/F290LP. The total exposure time

<sup>1</sup> <https://webbtelescope.org/contents/news-releases/2022/news-2022-035>

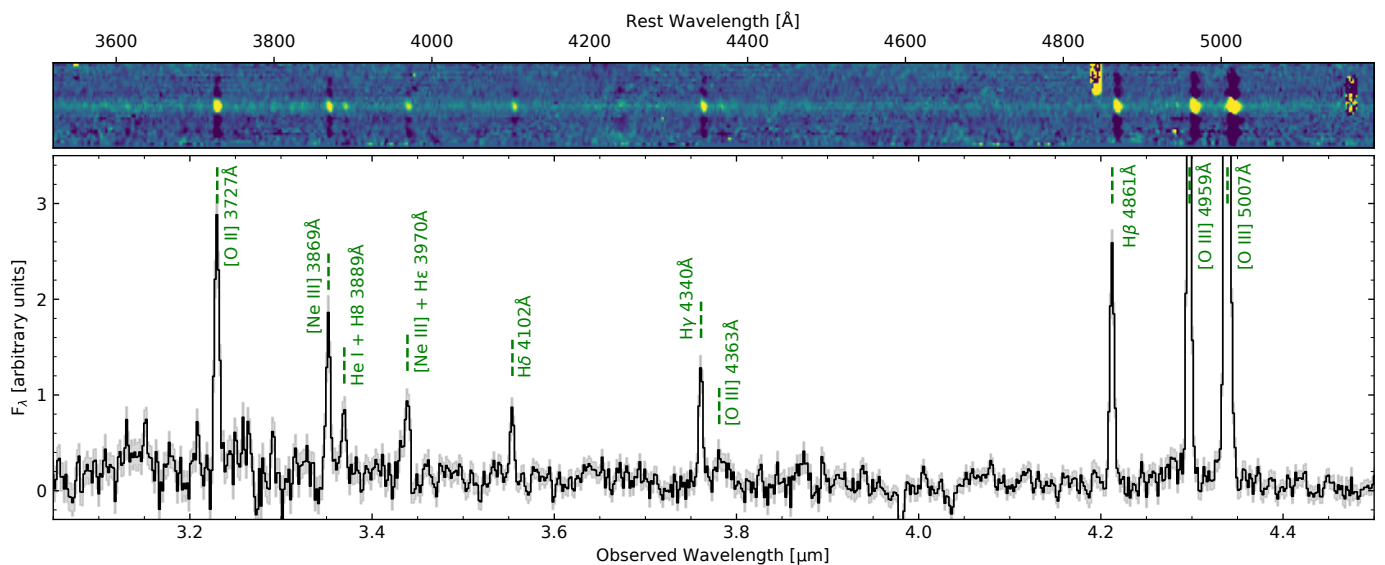


**Fig. 1.** 2D (top) and 1D (bottom) NIRSpec/JWST spectrum of 06355 at  $z = 7.664$  (black) and  $1\sigma$  uncertainty (grey). Vertical dashed lines mark the position of well-detected nebular emission lines. The continuum emission is also detected as seen in the 2D spectrum. X-axis in the bottom and top panels refer to the observed ( $\mu\text{m}$ ) and rest-frame wavelengths ( $\text{\AA}$ ), respectively.

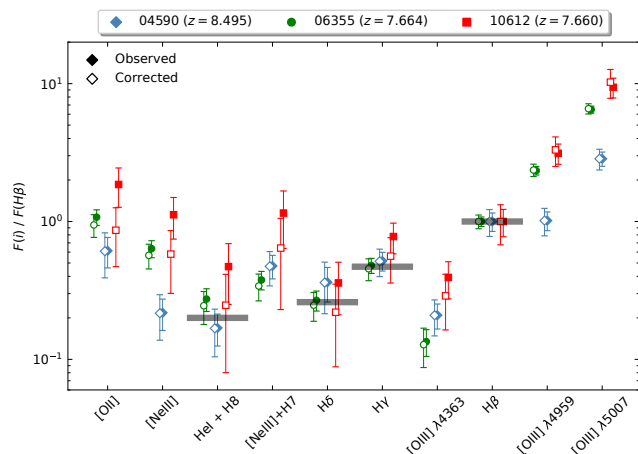


**Fig. 2.** Relative line intensities of the measured lines with respect to  $H\beta$ . Full and open symbols show the ratios prior to and after applying our flux correction (see text).

is  $2 \times 8754$  seconds for each grating/filter. This provides a spectral resolution  $R \approx 1000$  and a continuous spectral coverage of  $\approx 1.75 - 5.20 \mu\text{m}$ . Fully calibrated spectra (calibration level 3) were retrieved from the Mikulski Archive for Space Telescopes<sup>2</sup>, which were previously processed with the JWST Science Calibration Pipeline (CAL\_VER: 1.5.3 and CRDS\_CTX: jwst-0916.pmap). For each source, two individual 1D spectra (s007 and s008) are combined using the average flux, and after masking spectral regions affected by cosmic rays and other artifacts, after inspection of the 2D spectra. For 04590 we exclude data above  $\lambda_{\text{obs}} \geq 4.5 \mu\text{m}$  (i.e., after the detector gap) for the observation s008 as the 2D spectrum in this region shows several artifacts that might compromise the flux calibration, including a considerable flux gradient along the spatial direction. An example of the combined spectrum of 06355 at  $z \approx 7.7$  is shown in Fig. 1.

The spectra of the three sources show nebular emission lines, many of them detected with high significance ( $> 3\sigma$ ). These in-

clude Balmer lines ( $H\beta$ ,  $H\gamma$ ,  $H\delta$ ),  $[O \text{ II}]$  and  $[O \text{ III}]$ ,  $[Ne \text{ III}]$ , and  $He \text{ I}$ . In particular, the auroral  $[O \text{ III}] \lambda 4363$  line – key for accurate determinations of the O/H abundance using the direct method – is detected in all galaxies with a significance of  $3.9 - 5.7\sigma$ . Gaussian profiles are fitted to each line using the Python non-linear least-squares function CURVE-FIT, and assuming a constant level for the continuum (in  $f_\lambda$ ). We derive the redshifts for these sources using the brightest lines, namely  $H\gamma$ ,  $H\beta$ , and  $[O \text{ III}] \lambda \lambda 4959, 5007$  lines (Table 1). The continuum is clearly detected in the two  $z \approx 7.7$  sources (10612 and 06355, see Fig. 1) allowing the determination of the equivalent widths of the lines (Table 1). However, these do not include any correction for slit-losses and other possible effects due to different morphologies of the continuum emission and nebular lines.

After careful inspection of the flux measurements we noticed that some line ratios have nonphysical values, suggesting systematics on the flux calibration and throughput in the current JWST pipeline. For example, the observed Balmer line ratios are found to be larger than the intrinsic  $H\gamma/H\beta$  and  $H\delta/H\beta$  ratios assuming case B recombination. Before more accurate calibration reference files are available, we overcame this issue by applying an ad hoc correction to the flux calibration. More specifically, we fit a power law ( $\propto \lambda^\alpha$ ) to i) the intrinsic  $H\gamma/H\beta = 0.47$ ,  $H\delta/H\beta = 0.26$  (case B), and  $(He \text{ I} + H8)/H\beta = 0.2$  and to ii) the observed line ratios. The correction factor as a function of wavelength is thus given by the division between i) and ii) for each source, and it is applied to the full spectral range covered by the G235M/F170LP grating/filter configuration. This empirical correction results in a maximum increase of  $\sim 20 - 50\%$  (depending on galaxy) for the  $O32 = [O \text{ III}] \lambda 5007 / [O \text{ II}] \lambda 3727$  ratio, and smaller corrections for other line ratios. By doing this, we are also applying a first-order correction to the Balmer decrement, thus losing the information on the dust attenuation. Given the uncertainties on the flux calibration and on our empirical correction, we conservatively add 20% of uncertainties on our flux measurements, which should also account for other sources of uncertainty, such as those arising from the estimation of the continuum level. This depends on the different assumptions (e.g., size of the spectral windows used in the fit, constant level or straight line, noise fluctuations, etc.) and may affect the flux mea-

<sup>2</sup> <https://mast.stsci.edu/>

measurements of different lines. The measured line ratios, prior to and after correction, are shown in Fig. 2. Where possible, our analysis will focus mostly on lines ratios between nearby lines (see Section 3), thus minimizing possible issues on the flux calibration, and dust attenuation.

It must be noted that presently the data reduction is still in a preliminary stage, which uses in particular pre-launch calibration files (Rigby et al. 2022). To tackle with these limitations, different groups have used different approaches, including observations of a standard star, different extractions of the 2D spectra, different combinations of the 2 visits and other corrections (cf. Curti et al. 2022; Rhoads et al. 2022; Trump et al. 2022). A comparison shows differences in several line ratios, by amounts which are sometimes larger than the quoted uncertainties. To illustrate this, we subsequently compare our measurements with those from Curti et al. (2022) who have improved the calibration using a standard star. For other comparisons see also Taylor et al. (2022) and Brinchmann (2022).

## 2.2. JWST NIRC*am* observations

We make use of a single NIRC*am* pointing in the six wide filters F090W, F150W, F200W, F277W, F356W, and F444W, with a uniform exposure time of 2.1hr in each, and shallower NIRISS imaging in F115W. We obtained the calibrated and distortion-corrected NIRC*am* and NIRISS images from the publicly available reduction by Brammer (2022). The images were processed with the standard JWST pipeline up to stage 2b, before they were WCS aligned and combined with the `grizli`<sup>3</sup> pipeline (see Brammer et al., in prep). The images were pixel aligned at 40mas pixel scales, before producing a multi-wavelength catalog with SExtractor (Bertin & Arnouts 1996). Fluxes are measured in small circular apertures of 0'':32 diameter and corrected to total fluxes using the AUTO fluxes from the F200W detection image.

To determine stellar masses, SED fits to the 7 bands were done using the latest versions of the CIGALE and Prospector codes (Boquien et al. 2019; Johnson et al. 2021), exploring a relatively wide range of priors. Prior to correction for magnification, we find masses of  $\log(M_*/M_\odot) \sim 8.9 - 9.2$  and significant differences between the codes. We also note that the masses derived by Carnall et al. (2022) are systematically lower than ours, which should mainly be due to consistently younger ages found by these authors. Before more detailed analyses of the SEDs and spectra of these galaxies become available, we adopt the stellar masses from our preferred CIGALE fits and a conservative uncertainty of  $\pm 0.3$  (see Table 1). To correct the masses for gravitational magnification from the cluster, we use the magnification factors  $\mu$  from the lens models of Caminha et al. (2022). Other lens models, e.g. those used by Carnall et al. (2022), yield similar magnifications (differences of 10-50% at most) for the sources studied here.

## 2.3. Comparison samples

For comparison with low- $z$  galaxies we use a sample of 5607 star-forming galaxies from the SDSS Data Release 14 compiled by Y. Izotov and collaborators, analysed in earlier publications (e.g. Guseva et al. 2019; Ramambason et al. 2020). The selection criteria used for the extraction of star-forming galaxies are presented in Izotov et al. (2014). Then we require a detection of the [O III] $\lambda$ 4363 line with an accuracy better than  $4\sigma$ , allow-

ing thus direct abundance determinations using the  $T_e$ -method. Subsequently we refer to this sample as Izotov-DR14.

We also use the spectra of 89 galaxies at  $z \sim 0.3$  from the Low- $Z$  Lyman Continuum Survey (LzLCS), the first large sample of galaxies with UV spectroscopy covering both the Lyman continuum and non-ionizing UV (see Flury et al. 2022a,b). Approximately half of the sample has [O III] $\lambda$ 4363 detections.

## 3. Observed and derived properties of the $z \sim 8$ galaxies

### 3.1. Emission line properties

First we examine the observed emission line ratios in the three high- $z$  galaxies and compare them to those of the low- $z$  samples (cf. above). Figure 3 shows the main line ratios including the lines of [Ne III] $\lambda$ 3869, [O II] $\lambda$ 3727, [O III] $\lambda$ 4363, [O III] $\lambda$ 5007, and H $\gamma$ , which are detected in the JWST spectra. The [Ne III]/[O II] (Ne3O2) ratio is well known to closely trace O32, since both high ionization lines of [Ne III] and [O III] originate in the same zone of the HII region. Our measurements in the high- $z$  galaxies (and those from Curti et al. 2022, shown for comparison) are compatible with the observed correlation, providing confidence for our empirical flux calibration. By these line ratios, the three high- $z$  galaxies are found at relatively high excitation, corresponding to the tail of the distribution in low- $z$  compact star-forming galaxies (cf. Izotov et al. 2021a). Compared to the low- $z$  samples, the intensity of [O III] $\lambda$ 4363 is also found to be relatively high, with [O III] $\lambda$ 4363/H $\gamma \sim 0.3 - 0.5$ , as illustrated in Fig. 3. The highest- $z$  source (04590) is a bit offset towards low [O III] $\lambda$ 5007/[O III] $\lambda$ 4363.

The detection of the auroral [O III] $\lambda$ 4363 line and [O III] $\lambda$ 5007 provides access to the electron temperature  $T_e$ , and thus allows abundance determinations using the so-called ‘‘direct method’’ (see e.g. Kewley & Dopita 2002). To do this we follow the prescriptions of Izotov et al. (2006) assuming low densities. The results are listed in Table 1. We find electron temperatures  $T_e(\text{O}^{2+}) \sim 16000 - 18000$  K for the two  $z = 7.7$  galaxies, and nebular O/H abundances of  $12 + \log(\text{O}/\text{H}) \approx 7.86 - 7.88$  for the two objects. This includes both ionic abundances of O<sup>+</sup> and O<sup>2+</sup>, determined from the optical lines; in both cases O<sup>2+</sup> dominates. For 04590 the unusually low [O III] $\lambda$ 5007/[O III] $\lambda$ 4363 ratio leads to unphysically high electron temperatures ( $T_e \sim 35$  kK) and in excess of the highest accurate electron temperatures measured for star-forming galaxies at low- $z$  ( $T_e = 24800 \pm 900$  K, Izotov et al. 2021b). This result is consistently found by all other papers who have analysed the JWST, and some authors have derived electron temperatures as high as  $T_e = 37200 \pm 9900$  K (Rhoads et al. 2022). Although the detection of the [O III] $\lambda$ 4363 line is beyond doubt, we consider that better data will be needed before the electron temperatures can accurately be determined. Therefore the direct metallicity determinations for these high- $z$  galaxies should presently be taken with caution.

Different metallicity estimates can be obtained for the  $z = 8.495$  galaxy 04590 (see Table 1): From their finding of  $T_e \geq 20$  kK, Trump et al. (2022) conclude that  $12 + \log(\text{O}/\text{H}) < 7.69$  ( $< 1/10$  solar), from the empirical relation between  $T_e$  and  $12 + \log(\text{O}/\text{H})$  (cf. Pérez-Montero et al. 2021). Since standard strong line methods are not applicable at such low metallicities and for objects with ‘‘extreme’’ line ratios, we can, e.g., use the empirical calibration of Izotov et al. (2021b) based on measurements of R23<sup>4</sup> and O32, and which has been established

<sup>3</sup> <https://github.com/gbrammer/grizli/>

<sup>4</sup>  $R23 = ([\text{O III}] \lambda\lambda 4959, 5007 / \text{H}\beta + [\text{O II}] \lambda 3727 / \text{H}\beta)$

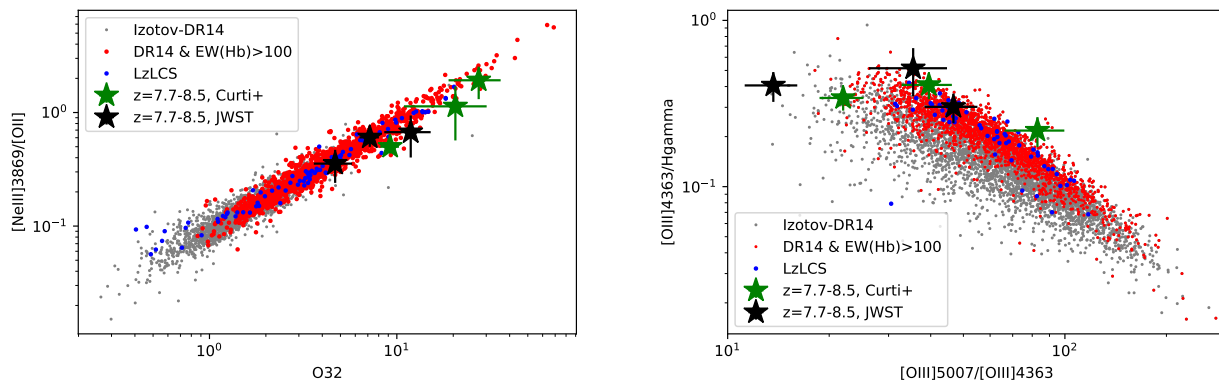


**Fig. 3.** Observed Ne3O2 ratio versus O32 (left panel) and  $[\text{O III}]\lambda 4363/\text{H}\gamma$  versus  $[\text{O III}]\lambda 5007/[\text{O III}]\lambda 4363$  (right panel) for the  $z \sim 8$  galaxies (black stars: our measurements; green stars: data from Curti et al. (2022)), the Izotov-DR14 sample of star-forming galaxies (grey and red points, according to  $\text{EW}(\text{H}\beta) < 100 \text{ \AA}$  and  $> 100 \text{ \AA}$ , respectively), and the LzLCS sample (blue points).

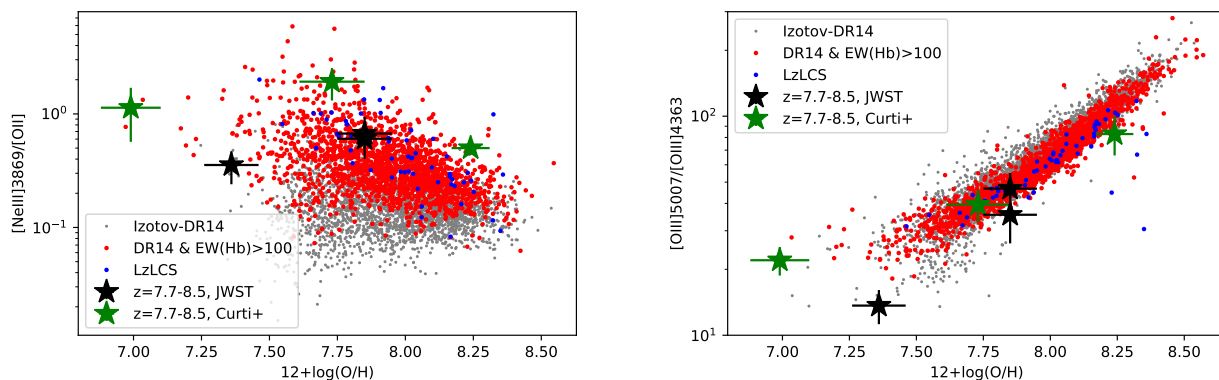


**Fig. 4.**  $[\text{Ne III}]\lambda 3869/[\text{O II}]\lambda 3727$  ratio (left panel) and intensity of the auroral  $[\text{O III}]\lambda 4363$  line relative to  $[\text{O III}]\lambda 5007$  (right panel), as a function of O/H. Same symbols as in Fig. 3.

at  $12 + \log(\text{O}/\text{H}) < 7.5$ . For 04590 we find  $12 + \log(\text{O}/\text{H}) = 7.39$  with our measurements, and  $12 + \log(\text{O}/\text{H}) = 7.24$  using the line ratios reported by Curti et al. (2022), who derived  $12 + \log(\text{O}/\text{H}) = 6.99 \pm 0.11$  by the direct method. With the measurements from Rhoads et al. (2022) we obtain an intermediate metallicity,  $12 + \log(\text{O}/\text{H}) = 7.30$ , using the same calibration. All studies so far agree that 04590 shows the lowest metallicity among the three  $z \sim 8$  galaxies.

In Fig. 4 we show the Ne3O2 and  $[\text{O III}]\lambda 4363/\text{H}\gamma$  ratios as a function of metallicity for the low- $z$  samples and the three  $z \sim 8$  galaxies. We use these line ratios which are close in wavelengths to minimize possible uncertainties of the flux calibration, differential slit losses and others. Empirically, these line ratios can also provide a simple estimate of the metallicity O/H, as discussed by earlier studies (see e.g. Nagao et al. 2006; Sanders et al. 2020). In any case, we see that our metallicity estimates of the high- $z$  galaxies lead to fairly compatible locations in these diagrams. We conclude that the three  $z \sim 8$  star-forming galaxies have low metallicities, in the range of  $12 + \log(\text{O}/\text{H}) \sim 7.4 - 8.0$ . More accurate determinations and a proper evaluation of the uncertainties await overall better data, including higher S/N data, proper calibrations, a more sophisticated data reduction, and continuum and line flux extractions.

Since the continuum is also detected in the NIRSPEC spectra of the two  $z = 7.7$  galaxies, and very weakly so also in the third object, we have also measured the  $[\text{O III}]$  equivalent width

(see Table 1). We compare our measurements with those from the low- $z$  galaxies in Fig. 5, where strong correlations between  $\text{EW}([\text{O III}]\lambda 5007)$  and properties such as O32, Ne3O2, and others have been found (Tang et al. 2019; Izotov et al. 2021a). Possibly, the high- $z$  sources are somewhat offset. In any case, the EWs are high in the galaxies with significant continuum detections, with  $\text{EW}([\text{O III}]\lambda 5007) \sim 700 \text{ \AA}$  in the brightest source.

Empirically, the ionizing photon production efficiency,  $\xi_{\text{ion}}$ , is found to increase with the  $[\text{O III}]\lambda 5007$  equivalent width, as also shown in Fig. 5. Using the relations found at low- $z$  and  $z \sim 1 - 2$  (see Tang et al. 2019; Izotov et al. 2021a), we estimate  $\log(\xi_{\text{ion}}) \approx 25.1 - 25.5 \text{ erg}^{-1} \text{ Hz}$ , up to a factor  $\sim 2$  higher than the “canonical” value often assumed in ionizing photon budget calculations (Robertson et al. 2013). This is comparable to other estimates of  $\xi_{\text{ion}}$  at high redshift (e.g. Stefanon et al. 2022).

### 3.2. Physical properties of the $z \sim 8$ galaxies and the mass-metallicity relation

As discussed, the three  $z \sim 8$  galaxies show emission line properties comparable to compact star-forming galaxies at low- $z$  with strong emission lines. Izotov et al. (2021a) have shown that the low- $z$  galaxies with strong lines ( $\text{EW}(\text{H}\beta) > 100 \text{ \AA}$ ) are good analogues of many of the  $z \sim 1 - 3$  star-forming galaxies (Lyman alpha emitters and Lyman break galaxies) studied so far. By in-

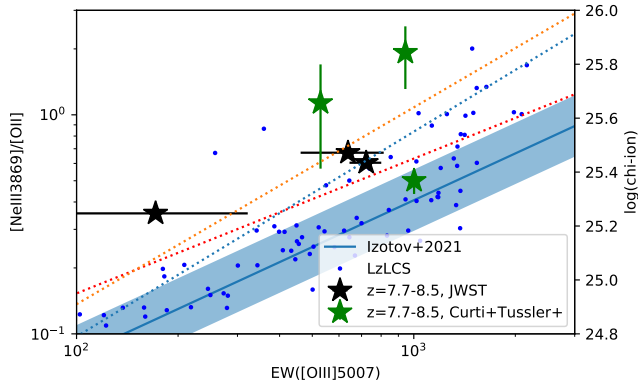


**Fig. 5.** Relation between the observed Ne3O2 ratio (left y-axis),  $\xi_{\text{ion}}$  (right y-axis), and  $\text{EW}([\text{O III}]\lambda 5007)$ . The  $z \sim 8$  galaxies are marked with black stars for our measurements and green stars using the line ratios and equivalent widths taken from Curti et al. (2022) and Trussler et al. (2022) respectively. The shaded stripe shows the mean Ne3O2–EW relation and scatter in the large low- $z$  sample of Izotov et al. (2021a). The dotted lines show the relations between  $\xi_{\text{ion}}$  (right axis) and  $\text{EW}([\text{O III}]\lambda 5007)$  found at  $z \sim 0 - 1$  (Chevallard et al. 2018; Izotov et al. 2021a).

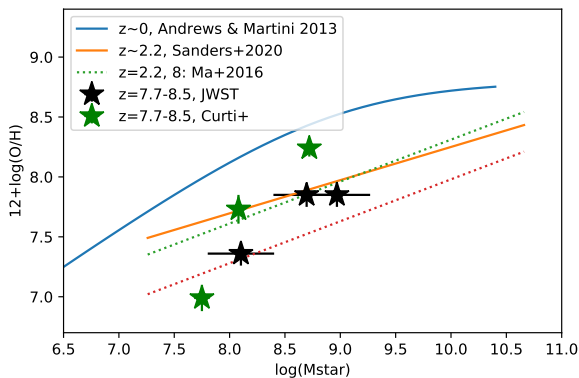


**Fig. 6.** Mass-metallicity relation of the three  $z \sim 8$  galaxies (black stars) compared to mean relations observed at  $z = 0$  and 2.2 (Andrews & Martini 2013; Sanders et al. 2020), and results from numerical simulations at  $z = 2.2$  and 8 (dotted lines) from Ma et al. (2016). Green stars show the results from adopting stellar masses determined by Curti et al. (2022), who quote very small uncertainties for their stellar masses.

ference the emission line properties of the three  $z \sim 8$  galaxies studied here therefore also resemble those at intermediate redshifts.

By construction, the galaxies selected here cannot be claimed to be “typical”, and larger, systematic studies will be needed. From our measurements, one object (10612) shows a very high ratio  $[\text{O III}]\lambda 5007/\text{H}\beta \approx 10$  and a strong  $[\text{O III}]\lambda 4363$  line, which could indicate an active galaxy (Seyfert 2, see also Brinchmann 2022; Curti et al. 2022). On the other hand, we clearly find evidence for one star-forming galaxy with a fairly low metallicity (04590 with  $12 + \log(\text{O}/\text{H}) \approx 7.2 - 7.4$ ).

If we combine our nebular metallicity estimates with the stellar masses described earlier, we obtain the mass-metallicity relation shown in Fig. 6. Our objects are found close to or below the mass-metallicity relation observed at  $z \sim 2$  and possibly offset by  $\sim 0.2 - 0.3$  below this relation, in good agreement with the relation derived by Ma et al. (2016) from simulations. Similar re-

**Table 1.** Observed and derived quantities for the three high- $z$  galaxies

Quantity	04590	06355	10612
redshift $z$	8.495	7.664	7.660
$T_e(\text{OIII})$		15584	18146
$12 + \log(\text{O}/\text{H})^a$		7.86	7.88
$12 + \log(\text{O}/\text{H})^b$	7.50	7.85	8.0
$12 + \log(\text{O}/\text{H})^c$	7.39	7.76	7.91
O32	7.0	6.3	10.6
$\text{EW}([\text{O III}]\lambda 5007)$	$172 \pm 150$	$723 \pm 78$	$638 \pm 176$
$m_{F277W}$	27.8	26.6	25.6
$M_{1500}^d$	-20.29	-21.09	-20.38
$M_{1500}^e$	-18.06	-20.51	-19.81
$\beta_{1500}$	$-2.20 \pm 0.15$	$-1.96 \pm 0.22$	$-2.31 \pm 0.11$
$\log(M_\star) \times \mu$	$9.0 \pm 0.3$	$9.2 \pm 0.3$	$8.9 \pm 0.3$
Magnification $\mu$	7.9	1.7	1.7

<sup>a</sup> direct method, <sup>b</sup> assuming  $T_e = 16000$  K

<sup>c</sup> using strong line methods (Izotov+2019,2021)

<sup>d</sup> observed, including lensing

<sup>e</sup> corrected for lensing

sults were also obtained by Jones et al. (2020) using an indirect method based on ALMA emission line detections. However, at the present stage we consider the stellar masses uncertain, since these depend significantly on assumptions of the star formation history and on the age of stellar populations (see also Tang et al. 2022), plus uncertainties with the zeropoints of NIRCcam (see Rigby et al. 2022). For example, comparing the masses derived from SEDs by Carnall et al. (2022), Curti et al. (2022), and our work, we can see significant differences which are generally larger than the uncertainties cited. Adopting the lower masses from Carnall et al. (2022), e.g., which would imply that our  $z \sim 8$  galaxies lie close to the  $z \sim 2$  mass-metallicity relation. The lower masses are mostly due to the very young ages ( $\sim 1 - 2$  Myr) inferred by these authors, whereas our SED fits favour less extreme populations. Although Carnall et al. (2022) claim that the SEDs show evidence for Balmer jumps (i.e. Balmer breaks in emission due to strong nebular continuum), we do not see such a behaviour in the NIRSspec spectrum of the brightest source, 06355, shown in Fig. 1.

Having shown that the  $z \sim 8$  galaxies closely resemble strong emission line galaxies from our low- $z$  sample it is tempting to infer indirectly other properties using correlations established at low- $z$ . Certainly, the high O32 ratios, low metallicity, and blue UV slopes ( $\beta$ ) suggest that these galaxies could contribute to cosmic reionization, i.e. have escaping ionizing photons. For example, for the observed values of O32,  $12 + \log(\text{O}/\text{H})$ , and  $\beta$ , the LzLCS results suggest a 30-60% detection fraction of the Lyman continuum. Adopting the mean relation between the LyC escape fraction,  $f_{\text{esc}}$ , and the UV slope, we estimate  $f_{\text{esc}} = 0.03 - 0.08$  for the three  $z \sim 8$  galaxies, although the LyC escape could also be significantly higher (see Chisholm et al. 2022).

Future improvements in the calibration and data reduction and additional observations will allow us to determine more accurately equivalent widths and total line fluxes of emission lines, measure continuum shapes, combine photometry and spectra etc. and hence improve our knowledge of the physical properties of galaxies at high-redshift.

## 4. Conclusion

We have analysed the rest-frame optical spectra of two galaxies at  $z = 7.7$  and one at  $z = 8.5$  from the JWST Early Release

Observations. The spectra, exhibit numerous emission lines of H, He I, [O II], [O III], and [Ne III], as commonly seen in metal-poor star-forming galaxies at low redshift. They provide, for the first time in the epoch of reionization, detailed information on the chemical composition and interstellar medium of these galaxies. Our main results are summarized as follows:

- The auroral [O III] $\lambda$ 4363 line is significantly detected in all galaxies with  $3.9 - 5.7\sigma$ , allowing the determination of the O/H abundance (metallicity) using the direct method. With this method and different strong-line methods we estimate metallicities between  $12 + \log(\text{O}/\text{H}) = 7.4 - 8.0$ , i.e.  $\sim 5 - 20\%$  of solar.
- All three galaxies show a high excitation, as measured by their line ratios of  $\text{O32} = 6 - 11$  and  $\text{Ne3O2} = 0.4 - 0.7$ , or even higher, according to Curti et al. (2022) and Rhoads et al. (2022). The observed emission line ratios are similar to those of rare low- $z$  star-forming galaxies, which are considered analogues of high-redshift ( $z \sim 1 - 3$ ) galaxies. One of the  $z = 7.6$  galaxies shows unusually high  $[\text{O III}]\lambda 5007/\text{H}\beta \approx 10$ , possibly indicative of nuclear activity (Seyfert 2).
- The  $z \sim 8$  galaxies show quite high equivalent widths, e.g.  $\text{EW}([\text{O III}]\lambda 5007)$  up to  $\sim 700 \text{ \AA}$ , as expected from low- $z$  galaxies with high excitation. Such galaxies are known to be efficient producers of ionizing photons. We conservatively estimate  $\log(\xi_{\text{ion}}) \sim 25.2 - 25.5 \text{ erg}^{-1} \text{ Hz}$  for our galaxies.
- Using stellar mass estimates from SED fits, we find the  $z \sim 8$  galaxies to lie close to or below the mass-metallicity relation (MZR) at  $z \sim 2$ . To assess if the MZR continues to evolve from  $z = 2$  to 8 will need future studies of larger galaxy samples and accurate metallicity determinations.

Overall, the first analysis of the rest-frame optical spectra of galaxies at  $z \sim 8$  indicates that the emission lines properties of galaxies in the epoch of reionization resemble those of relatively rare “local analogues” previously studied from the SDSS, and for which numerous physical properties have already been determined. These low- $z$  samples will soon be rivaled by numerous measurements with NIRSPEC onboard JWST. Clearly, the first data release reveals already an extremely promising “pre-view” of upcoming science with JWST in the early Universe. More robust inferences will require better data, including higher S/N spectra and improvements in the calibration, data reduction, and continuum and line flux extractions.

*Acknowledgements.* We are very grateful to the ERO and other teams who made these JWST observations possible. The Early Release Observations and associated materials were developed, executed, and compiled by the ERO production team: Hannah Braun, Claire Blome, Matthew Brown, Margaret Carruthers, Dan Coe, Joseph DePasquale, Nestor Espinoza, Macarena Garcia Marin, Karl Gordon, Alaina Henry, Leah Hustak, Andi James, Ann Jenkins, Anton Koekemoer, Stephanie LaMassa, David Law, Alexandra Lockwood, Amaya Moro-Martin, Susan Mullally, Alyssa Pagan, Dani Player, Klaus Pontoppidan, Charles Proffitt, Christine Pulliam, Leah Ramsay, Swara Ravindranath, Neill Reid, Massimo Robberto, Elena Sabbi, Leonardo Ubeda. The EROs were also made possible by the foundational efforts and support from the JWST instruments, STScI planning and scheduling, and Data Management teams. We acknowledge support from the Swiss National Science Foundation through project grant 200020\_207349 (PAO, LB). The Cosmic Dawn Center (DAWN) is funded by the Danish National Research Foundation under grant No. 140. Cloud-based data processing and file storage for this work is provided by the AWS Cloud Credits for Research program. Y.I. and N.G. acknowledge support from the National Academy of Sciences of Ukraine by its priority project No. 0122U002259 “Fundamental properties of the matter and its manifestation in micro world, astrophysics and cosmology”.

## References

Ahumada, R., Prieto, C. A., Almeida, A., et al. 2020, *ApJS*, 249, 3

- Andrews, B. H. & Martini, P. 2013, *ApJ*, 765, 140
- Arellano-Córdova, K. Z., Berg, D. A., Chisholm, J., et al. 2022, arXiv e-prints, arXiv:2208.02562
- Bertin, E. & Arnouts, S. 1996, *A&AS*, 117, 393
- Boquien, M., Burgarella, D., Roehlly, Y., et al. 2019, *A&A*, 622, A103
- Brammer, G. 2022, Images and catalogs of HST and JWST images in the SMACS-0723 field
- Brinchmann, J. 2022, arXiv e-prints, arXiv:2208.07467
- Caminha, G. B., Suyu, S. H., Mercurio, A., et al. 2022, arXiv e-prints, arXiv:2207.07567
- Carnall, A. C., Begley, R., McLeod, D. J., et al. 2022, arXiv e-prints, arXiv:2207.08778
- Chevallard, J., Charlot, S., Senchyna, P., et al. 2018, *MNRAS*, 479, 3264
- Chisholm, J., Saldana-Lopez, A., Flury, S., et al. 2022, arXiv e-prints, arXiv:2207.05771
- Curti, M., D’Eugenio, F., Carniani, S., et al. 2022, arXiv e-prints, arXiv:2207.12375
- Flury, S. R., Jaskot, A. E., Ferguson, H. C., et al. 2022a, *ApJS*, 260, 1
- Flury, S. R., Jaskot, A. E., Ferguson, H. C., et al. 2022b, *ApJ*, 930, 126
- Förster Schreiber, N. M. & Wuyts, S. 2020, *ARA&A*, 58, 661
- Guseva, N. G., Izotov, Y. I., Fricke, K. J., & Henkel, C. 2019, *A&A*, 624, A21
- Izotov, Y. I., Guseva, N. G., Fricke, K. J., & Henkel, C. 2014, *A&A*, 561, A33
- Izotov, Y. I., Guseva, N. G., Fricke, K. J., et al. 2021a, *A&A*, 646, A138
- Izotov, Y. I., Stasińska, G., Meynet, G., Guseva, N. G., & Thuan, T. X. 2006, *A&A*, 448, 955
- Izotov, Y. I., Thuan, T. X., & Guseva, N. G. 2021b, *MNRAS*, 504, 3996
- Johnson, B. D., Leja, J., Conroy, C., & Speagle, J. S. 2021, *ApJS*, 254, 22
- Jones, T., Sanders, R., Roberts-Borsani, G., et al. 2020, *ApJ*, 903, 150
- Katz, H., Saxena, A., Cameron, A. J., et al. 2022, arXiv e-prints, arXiv:2207.13693
- Kewley, L. J. & Dopita, M. A. 2002, *ApJS*, 142, 35
- Kewley, L. J., Nicholls, D. C., & Sutherland, R. S. 2019, *ARA&A*, 57, 511
- Kriek, M., Shapley, A. E., Reddy, N. A., et al. 2015, *ApJS*, 218, 15
- Ma, X., Hopkins, P. F., Faucher-Giguère, C.-A., et al. 2016, *MNRAS*, 456, 2140
- Nagao, T., Maiolino, R., & Marconi, A. 2006, *A&A*, 459, 85
- Pérez-Montero, E., Amorín, R., Sánchez Almeida, J., et al. 2021, *MNRAS*, 504, 1237
- Ramabason, L., Schaerer, D., Stasińska, G., et al. 2020, *A&A*, 644, A21
- Rhoads, J. E., Wold, I. G. B., Harish, S., et al. 2022, arXiv e-prints, arXiv:2207.13020
- Rigby, J., Perrin, M., McElwain, M., et al. 2022, arXiv e-prints, arXiv:2207.05632
- Robertson, B. E., Furlanetto, S. R., Schneider, E., et al. 2013, *ApJ*, 768, 71
- Sanders, R. L., Shapley, A. E., Reddy, N. A., et al. 2020, *MNRAS*, 491, 1427
- Stefanon, M., Bouwens, R. J., Illingworth, G. D., et al. 2022, *ApJ*, 935, 94
- Tang, M., Stark, D. P., Chevallard, J., & Charlot, S. 2019, *MNRAS*, 489, 2572
- Tang, M., Stark, D. P., & Ellis, R. S. 2022, *MNRAS*, 513, 5211
- Taylor, A. J., Barger, A. J., & Cowie, L. L. 2022, arXiv e-prints, arXiv:2208.06418
- Trump, J. R., Arrabal Haro, P., Simons, R. C., et al. 2022, arXiv e-prints, arXiv:2207.12388
- Trussler, J. A. A., Adams, N. J., Conselice, C. J., et al. 2022, arXiv e-prints, arXiv:2207.14265